



# Investigation of the feedback mechanism in ideally expanded round impinging jets using large-eddy simulation

Romain Gojon<sup>1,2,\*</sup> and Christophe Bogey<sup>1,†</sup>

1. *Laboratoire de Mécanique des Fluides et d'Acoustique*

*UMR CNRS 5506, Ecole Centrale de Lyon*

*69134 Ecully, France*

2. *Department of Mechanics, Royal Institute of Technology (KTH)*

*Linné FLOW Centre*

*Stockholm, Sweden*

Large-eddy simulations (LES) have been performed in order to study the tone generation mechanism in four supersonic ideally expanded round impinging jets. The jets have a Mach number of 1.5, and a Reynolds number of  $6 \times 10^4$ . They impinge normally on a flat plate located at a distance from the nozzle exit varying from  $6r_0$  up to  $12r_0$  where  $r_0$  is the jet nozzle radius. The aerodynamic properties of the jets are first investigated. In particular, the convection velocity of the turbulent structures in the jet shear layers is computed. In the spectra of pressure fluctuations in the vicinity of the nozzle exit, intense tones emerge. Their associated Strouhal numbers are in agreement with measurements available for round impinging jets with similar exit conditions. The tone frequencies also correspond well to the frequencies predicted by the classical model of the aeroacoustic feedback establishing between the nozzle lips and the flat plate. A study of the feedback mechanism is then proposed by applying Fourier decomposition to the near pressure fields. The feedback mechanism is found to lead to the formation of hydrodynamic-acoustic standing waves. Moreover, for each tone frequency, the corresponding axisymmetric or helical oscillation mode of the jet is examined. Finally, an analysis is conducted using a vortex sheet model of the jet in order to determine the allowable frequency ranges of the upstream-propagating neutral acoustic wave modes. The tone frequencies obtained in the LES fall within these ranges, depending on their axisymmetric or helical nature.

## I. Introduction

Jets impinging on a flat plate have been studied experimentally by many authors over the past sixty years. In some cases, very intense tones have been observed in the acoustic field. In his pioneering work, Powell<sup>1</sup> suggested that they are due to a feedback mechanism between hydrodynamic disturbances propagating downstream from the nozzle lips down to the plate and acoustic waves propagating upstream from the plate to the nozzle lips.

Subsonic round jets at exit Mach numbers between 0.3 and 0.9 impinging on a flat plate normally have been studied by Ho and Nosseir<sup>2</sup> and Nosseir and Ho<sup>3</sup> in the eighties, among others. These authors built a simplified model predicting the frequencies of the feedback mechanism based on cross-correlations between microphones. Supersonic round impinging jets have also been investigated experimentally by Henderson and Powell<sup>4</sup>, Krothapalli *et al.*<sup>5</sup> and Henderson *et al.*<sup>6</sup> and more recently by Risborg and Soria<sup>7</sup>, Buchmann *et al.*<sup>8</sup> and Mitchell *et al.*<sup>9</sup> using high-speed optical measurements. In some cases, a feedback mechanism similar to that encountered in subsonic jets was found. This mechanism happens very often when the jets are ideally

\*PhD, now PostDoc at KTH Mechanics, gojon@kth.se

†CNRS Research Scientist, AIAA Senior Member & Associate Fellow, christophe.bogey@ec-lyon.fr.

expanded, but less frequently and only for certain nozzle-to-plate distances when the jets are imperfectly expanded. Henderson *et al.*<sup>6</sup> suggested that in the latter case, the feedback loop establishes only when a Mach disk forms upstream from the plate. Recently, for ideally expanded jets, Davis *et al.*<sup>10</sup> studied the wall pressure oscillations on the plate using a fast-response Pressure-Sensitive Paint. Besides, for planar impinging jets, Norum<sup>11</sup> and Tam and Norum<sup>12</sup> obtained, in certain cases, acoustic spectra with two emerging tone frequencies. The lower and upper tone frequencies were respectively associated with varicose (symmetric) oscillation modes of the jets, and with sinuous (antisymmetric) oscillation modes. Similar tone frequencies were found in a 2-D simulation by Hourigan *et al.*<sup>13</sup> In order to explain the symmetric or antisymmetric nature of the jet oscillations, Tam and Norum<sup>12</sup> proposed that the upstream propagating waves of the feedback mechanism can be linked to the neutral acoustic wave modes of the vortex sheet model of the jet. They found an allowable frequency range for each of these modes and noted that the two emerging tones observed in the experiments of Norum<sup>11</sup> fall into the first symmetric and the first antisymmetric allowable ranges thus obtained, depending on the corresponding nature of the mode.

In the present work, the LES of four ideally expanded round jets impinging on a flat plate are carried out in order to investigate the feedback mechanism establishing between the nozzle lip of the jets and the plate. The jets are characterized by a Mach number of 1.5, and a Reynolds number of  $6 \times 10^4$ . They impinge normally on a plate located at a distance from the nozzle exit varying from  $6r_0$  up to  $12r_0$ . The aerodynamic and acoustic results are presented. In particular, the convection velocity of the turbulent structures in the jet shear layers is computed. The Strouhal numbers of the tones observed in the near acoustic fields are compared with measurements available for round jets with similar exit conditions and with the classical model of the aeroacoustic feedback mechanism. A study of the feedback mechanism is then proposed by applying Fourier decomposition to the near pressure fields, to discuss whether the feedback mechanism leads to the formation of hydrodynamic-acoustic standing waves. Moreover, for each tone frequency, the axisymmetric or helical oscillation mode of the jet is examined. An analysis is finally conducted using a vortex sheet model of the jet in order to determine the allowable frequency ranges of the upstream propagating neutral acoustic wave modes.

The paper is organized as follows. The jets parameters and the numerical methods used for the LES are given in section II. The aerodynamic properties of the jets are then presented in section III. The acoustic fields are analysed and compared with experimental data in the section IV. The tone frequencies produced by the aeroacoustic feedback mechanism are studied in section V by applying Fourier decomposition to the pressure field. Concluding remarks are given in section VI.

## II. Parameters

### II.A. Jets parameters

Large-eddy simulations are performed for four round jets impinging normally on a flat plate for nozzle-to-plate distances  $L$  of  $6r_0$ ,  $8r_0$ ,  $10r_0$ , and  $12r_0$ . The different cases are presented in table 1. They are referred to as JetL6, JetL8, JetL10 and JetL12, respectively. The jets originate from a pipe nozzle of diameter  $D$ , whose lip is  $0.1r_0$  thick. They are ideally expanded, and have a Mach number of  $\mathcal{M}_j = u_j/a_j = 1.5$  where  $u_j$  is the jet exit velocity and  $a_j$  is the speed of sound in the jet. Their Reynolds number is  $Re_j = u_j D/\nu = 6 \times 10^4$  where  $\nu$  is the kinematic molecular viscosity. The jet ejection conditions and the nozzle-to-plate distances are similar to those in the experimental study of Krothapalli *et al.*<sup>5</sup> Finally, a Blasius boundary-layer mean-velocity profile with a thickness of  $0.15r_0$  is imposed at the nozzle exit. Finally, vortical disturbances not correlated in the azimuthal direction<sup>14</sup> are added in the boundary layer in the nozzle at  $z = -r_0$  in order to generate velocity fluctuations at the nozzle exit.

	$\mathcal{M}_j$	$Re_j$	$L$
JetL6	1.5	$6 \times 10^4$	$6r_0$
JetL8	1.5	$6 \times 10^4$	$8r_0$
JetL10	1.5	$6 \times 10^4$	$10r_0$
JetL12	1.5	$6 \times 10^4$	$12r_0$

Table 1. Jet parameters: Mach number  $\mathcal{M}_j = u_j/a_j$ , Reynolds number  $Re_j = u_j D/\nu$  and nozzle-to-plate distance  $L$ .

## II.B. Numerical parameters

The LES are performed by using unsteady compressible Navier-Stokes equations on cylindrical meshes for which  $r$ ,  $\theta$  and  $z$  denote the radial, azimuthal and axial directions, respectively. An explicit six-stage Runge-Kutta algorithm is used for time integration, and low-dissipation and low-dispersion eleven-point explicit finite differences are used for spatial derivation<sup>15,16</sup>. At the end of each time step, a high-order filtering is applied to the flow conservative variables in order to remove grid-to-grid oscillations and to relax subgrid-scale turbulent energy. The radiation conditions of Tam and Dong<sup>17</sup> are implemented at the inflow and lateral boundaries of the computational domain. A sponge zone combining grid stretching and Laplacian filtering is also employed to damp the turbulent fluctuations before they reach the lateral boundaries. Adiabatic conditions are imposed to the nozzle wall and the flat plate. The present numerical set up has been applied in past work<sup>14</sup> to simulate round jets at a Mach number 0.9. In the present simulations, a shock-capturing filtering is applied in order to avoid Gibbs oscillations near shocks. It consists in applying a conservative second-order filter optimised in Fourier space at a magnitude determined each time step using a shock sensor<sup>18</sup>. This method was successfully used by Cacqueray *et al.*<sup>19</sup> for the LES of an overexpanded jet at an equivalent Mach number  $\mathcal{M}_j = 3.3$ . The axis singularity is treated with the method proposed by Mohseni and Colonius<sup>20</sup>. A reduction of the effective resolution near the origin of the polar coordinates is also implemented<sup>21</sup>, in order to increase the time step of the simulation. The simulations are carried out using an OpenMP-based in-house solver. A total of 100,000 iterations are computed in each case after the transient period. The simulation time is thus equal to  $250D/u_j$ .

The cylindrical meshes contain between 202 and 240 million points, as noted in table 2. The variations of the radial and axial mesh spacings are represented in figure 1. The meshes are very similar to those used in a previous study<sup>22</sup> for the simulations of underexpanded round impinging jets. Notably, the maximum mesh spacing of  $0.06r_0$  allow acoustic waves with Strouhal numbers up to  $St = fD/u_j = 6.1$  to be well propagated, where  $f$  is the frequency.

	$n_r$	$n_\theta$	$n_z$	$n_r \times n_\theta \times n_z$
JetL6	500	512	791	$202 \times 10^6$
JetL8	500	512	803	$205 \times 10^6$
JetL10	500	512	869	$222 \times 10^6$
JetL12	500	512	936	$240 \times 10^6$

Table 2. Mesh parameters: number of points  $n_r$ ,  $n_\theta$  and  $n_z$  in the radial, azimuthal and axial direction, and total number of points.

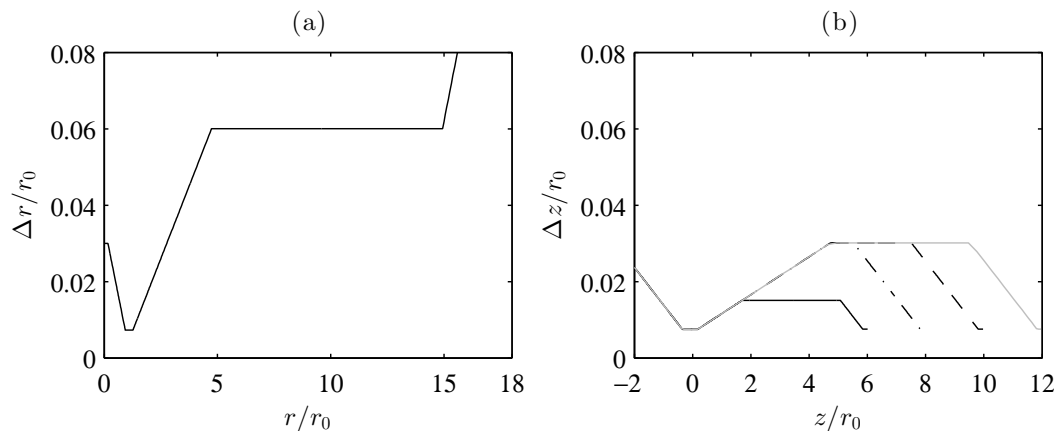
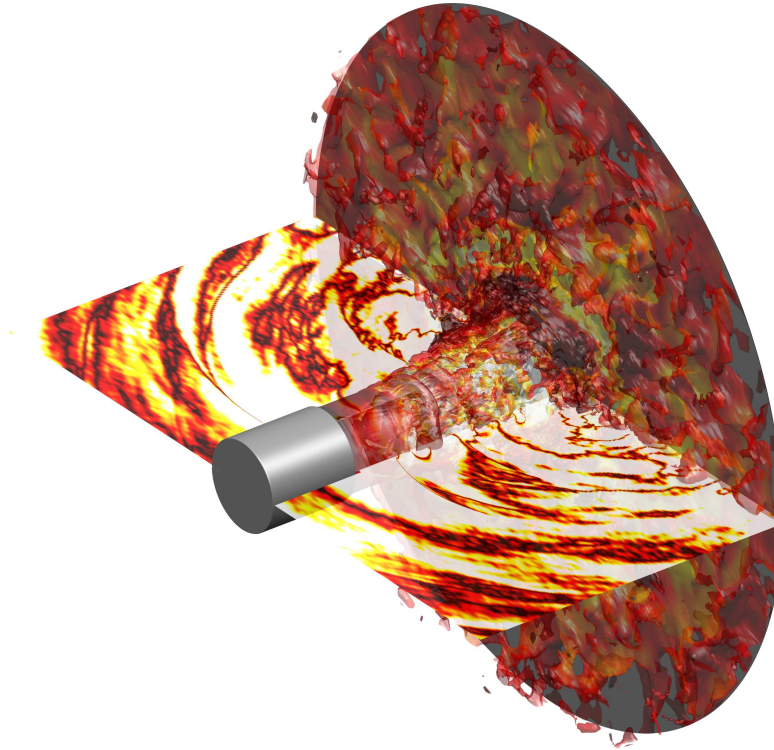


Figure 1. Representation of (a) the radial mesh spacings, and (b) the axial mesh spacings for — JetL6, - - - JetL8, - · - JetL10, and · · · JetL12.

### III. Aerodynamic results

#### III.A. Flow snapshots

In order to visualize simultaneously the jet flow and acoustic fields, three-dimensional snapshots are displayed in figures 2 and 3 for JetL6 and JetL10, respectively. The mixing layers of the jets are represented by isosurfaces of density. At the nozzle exit, the jets appear almost laminar. Downstream, for  $z > 2r_0$ , both small and large turbulent structures can be seen, in agreement with the Reynolds number of  $Re_j = 6 \times 10^4$ . The near acoustic fields of the jets in the plane  $\theta = 0$  are also shown. For the two jets, acoustic waves are clearly noted. They seem to be generated at the wall near the region of impact, and to propagate in the upstream direction. For JetL10, these waves are visibly symmetrically organised with respect to the jet axis. This could indicate an axisymmetric oscillation mode for the main tone frequency in this case.



**Figure 2.** Isosurfaces of density for JetL6. The isosurfaces for  $1.3 \text{ kg}\cdot\text{m}^{-3}$  are represented colored by the Mach number. The pressure field in the plane  $\theta = 0$  is also shown. The nozzle and the flat plate are in grey.

Snapshots of density and fluctuating pressure obtained for the present jets in the  $(z, r)$  plane are provided in figure 4. Isolated snapshots must be considered with caution but they provide qualitative results. For all cases, both small and large turbulent structures are observed in the shear layers of the jet. In the pressure fields, sound waves coming from the region of impact and propagating mostly in the upstream direction are visible. Their amplitudes seem to decrease with the nozzle-to-plate distance  $L$ . Moreover, for JetL8, JetL10 and JetL12, additional acoustic contributions consisting of circular wavefronts centered around  $z \simeq 3r_0$  in the jet shear layers and propagating in the lateral direction are seen. Given the temporal evolution of the jets, it seems that they are due to the interactions between the upstream propagating acoustic waves and the shear-layer turbulent structures.

#### III.B. Mean flow fields

The mean velocity fields obtained in the  $(z, r)$  plane are shown in figure 5. As expected, very small variations, of only around 3.5% of the jet exit velocity, are noticed near the axis, indicating that the jets are almost ideally expanded. In all cases, a stagnation point is visible on the plate at  $r = 0$  and a wall jet is created after the impact. The important parameters of wall jets are the maximum mean velocity  $u_{max}$ , the distance  $z_{max}$  from the wall at which the mean velocity reaches  $u_{max}$  and the distance  $z_{1/2}$  at which the velocity has dropped to  $u_{max}/2$ , refer to Irwin<sup>23</sup> and George *et al.*<sup>24</sup> for instance. For the present wall jets, the

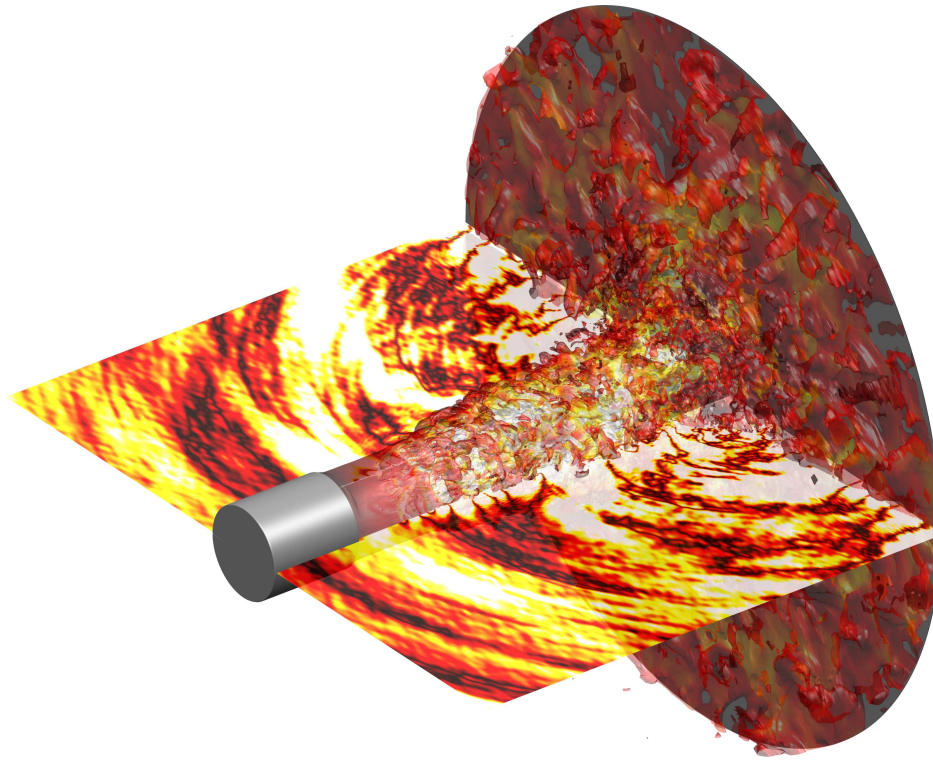


Figure 3. Isosurfaces of density for JetL10. The isosurfaces for  $1.3 \text{ kg}\cdot\text{m}^{-3}$  are represented colored by the Mach number. The pressure field in the plane  $\theta = 0$  is also shown. The nozzle and the flat plate are in grey.

values calculated at  $r = 2r_0$  are given in table 3. The maximum velocity of the wall jets decreases with the nozzle-to-plate distance, as expected. Simultaneously, the plane wall jet thickness  $z_{1/2}$  increases. The thickness  $z_{max}$  does not exhibit any clear behaviour.

	$u_{max} \text{ (m}\cdot\text{s}^{-1}\text{)}$	$z_{max}/r_0$	$z_{1/2}/r_0$
JetL6	385	0.077	0.41
JetL8	371	0.103	0.445
JetL10	362	0.105	0.464
JetL12	350	0.085	0.485

Table 3. Maximum velocities  $u_{max}$  and thicknesses  $z_{max}/r_0$  and  $z_{1/2}/r_0$  of the wall jets at  $r = 2r_0$ .

### III.C. Velocity fluctuations

The rms values of axial and radial velocity fluctuations  $u'$  and  $v'$  obtained for the four present jets are shown in figures 6 and 7, respectively. For the axial velocity, values of about 15% of the jet exit velocity are found in the shear layers of the jets. Peak values are observed approximately  $0.5r_0$  upstream of the plate, at  $r \simeq 0.8r_0$ . The maximum value around this location decreases from 20% down to 15% with increasing nozzle-to-plate distance. For the radial velocity, in figure 7, high rms values are found in the wall jets. The maximum values in these regions decreases with the nozzle-to-plate distance, from 25% of the jet exit velocity for JetL6 down to 15% for JetL12.

### III.D. Convection velocity

The evolution of the turbulent structures in the shear layers and more precisely their convection velocity are of primary concern to understand the feedback mechanism establishing between the nozzle and the plate. In this study, the convection velocity of the turbulent structures along the lipline at  $r = r_0$  are computed from cross-correlations of axial velocity fluctuations  $u'$ . The results are shown in figure 8. For the four

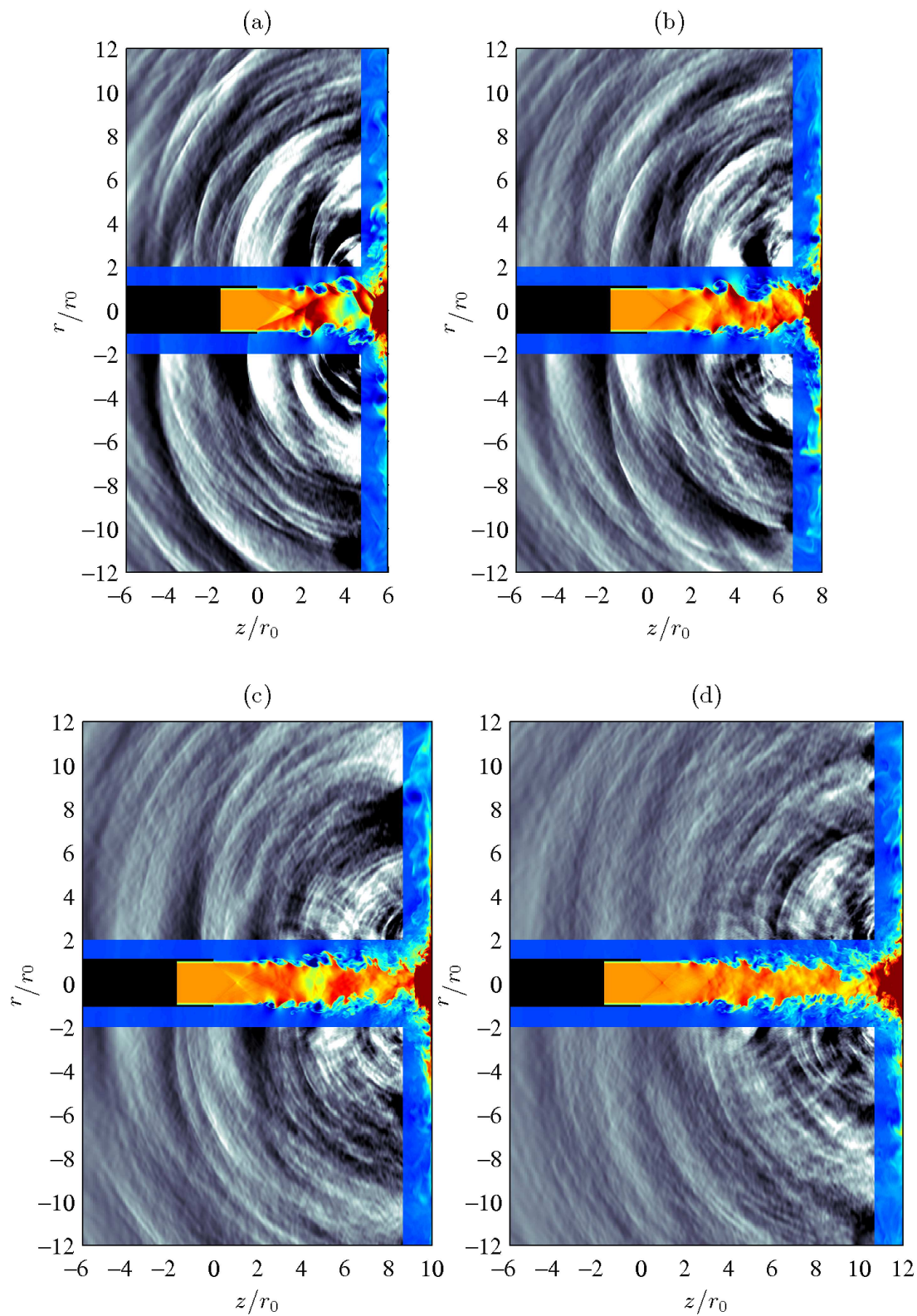


Figure 4. Snapshots in the  $(z, r)$  plane of the density in the jets and close to the flat plate and of the pressure fluctuations for (a) JetL6, (b) JetL8, (c) JetL10 and (d) JetL12. The colour scale ranges from 1 to 2  $\text{kg}\cdot\text{m}^{-3}$  for the density and from -5000 to 5000 Pa for the fluctuating pressure. The nozzle is in black.

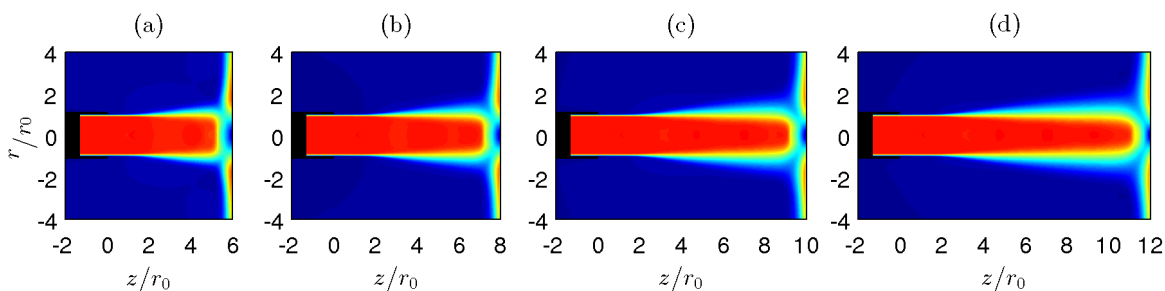


Figure 5. Mean velocity obtained in the  $(z, r)$  plane for (a) JetL6, (b) JetL8, (c) JetL10 and (d) JetL12. The colour scale ranges from 0 to  $500 \text{ m.s}^{-1}$ . The nozzle is in black.

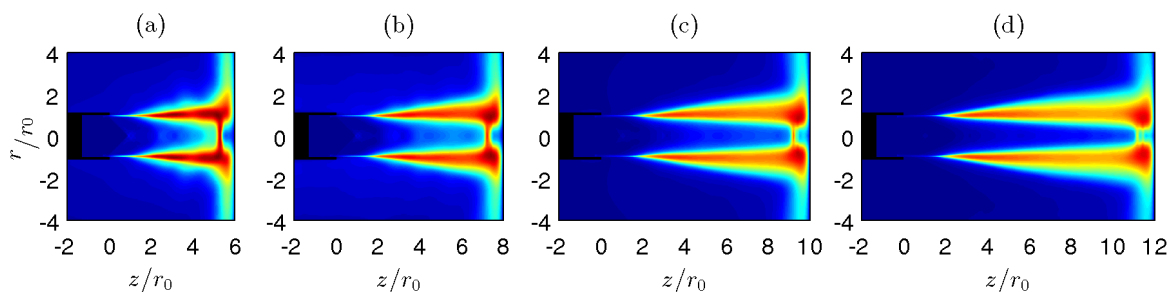


Figure 6. Rms values of axial velocity  $\langle u'_z u'_z \rangle^{1/2}$  obtained in the  $(z, r)$  plane for (a) JetL6, (b) JetL8, (c) JetL10 and (d) JetL12. The colour scale ranges from 0 to  $100 \text{ m.s}^{-1}$ . The nozzle is in black.

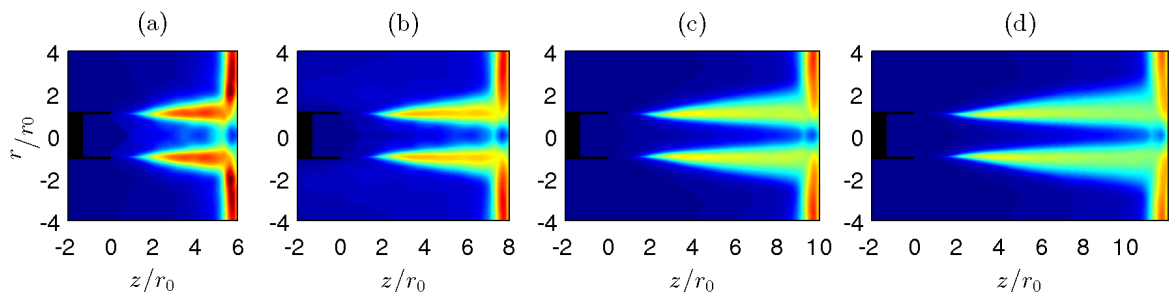


Figure 7. Rms values of radial velocity  $\langle u'_r u'_r \rangle^{1/2}$  obtained in the  $(z, r)$  plane for (a) JetL6, (b) JetL8, (c) JetL10 and (d) JetL12. The colour scale ranges from 0 to  $100 \text{ m.s}^{-1}$ . The nozzle is in black.

jets, the convection velocity is close to  $0.50u_j$  at  $z = 2r_0$ . Farther downstream, it increases, reaches a peak typically at two nozzle radii upstream from the plate, and then decreases. The maximal convection velocity is equal to about  $0.68u_j$  in all cases. Overall, the average convection velocity of the turbulent structures along the lipline is around  $0.60u_j$ . This value is slightly higher than the values between  $0.50u_j$  and  $0.60u_j$  found experimentally by Krothapalli *et al.*<sup>5</sup> for similar jets.

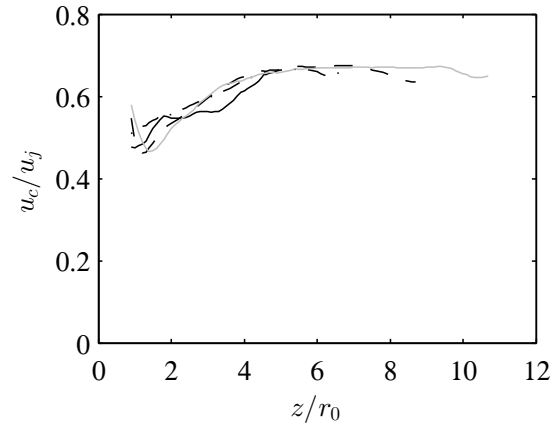


Figure 8. Convection velocity in the shear layers for — JetL6, ··· JetL8, - - - JetL10, and - · - JetL12.

## IV. Acoustic results

### IV.A. Pressure spectra

The pressure spectra obtained at  $z = 0$  and  $r = 2r_0$  are displayed in figure 9 as a function of the Strouhal number  $St$ . Several tones emerge in the four jets. A large number of tones were also observed experimentally by Norum<sup>11</sup> and by Krothapalli *et al.*<sup>5</sup> for rectangular and round ideally expanded impinging jets. Given the number of tones in the present jets, only the frequencies of those whose level is about 10 dB higher than the broadband noise level are considered. They are given in table 4.

	$St_1$	$St_2$	$St_3$	$S_4$
JetL6	0.345	<b>0.455</b>	0.69	0.80
JetL8	0.365	<b>0.445</b>	—	—
JetL10	0.29	<b>0.375</b>	0.44	0.665
JetL12	<b>0.305</b>	0.38	—	—

Table 4. Strouhal numbers emerging in the spectra of figure 9. The Strouhal numbers of the dominant tone for each jet appear in bold.

For JetL6, in figure 9(a), the tone frequencies are not the harmonics of one fundamental frequency. Instead, they are given by the linear combinations of the tone frequencies at Strouhal numbers  $St_1 = 0.345$  and  $St_2 = 0.455$ , yielding  $St_3 = 2St_1$  and  $St_4 = St_1 + St_2$ . It can also be noted that most of the secondary tones which are not reported in table 4 are also linear combinations of these two tones. A similar result was found by Tam and Norum<sup>12</sup> for supersonic ideally expanded rectangular impinging jets. Several tone frequencies were obtained in most cases, and for some distances, two tone frequencies and their linear combinations were observed. For JetL8, in figure 9(b), two dominant tones and several secondary tones are also noted. For JetL10, four dominant tones appear. The relation  $St_4 = St_1 + St_2$  can be seen. Finally, for JetL12, in figure 9(d), two dominant tone frequencies are visible.

### IV.B. Tone frequencies

In order to explain the tone frequencies found experimentally, Powell<sup>1</sup> was the first to suggest that a feedback mechanism establishes between the nozzle lips and the flat plate. This mechanism consists of two steps. First, in the shear layer, a turbulent structure is convected downstream from the nozzle to the plate. The structure

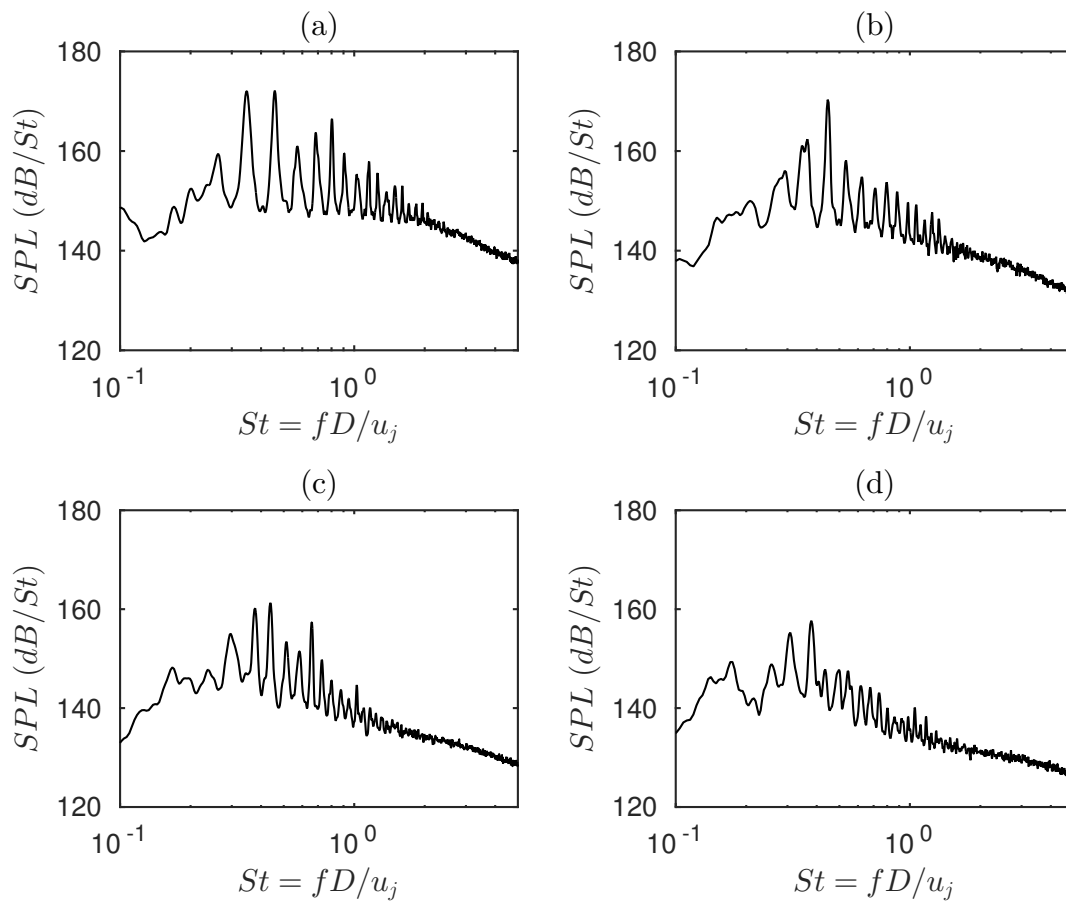


Figure 9. Pressure spectra obtained at  $z = 0$  and  $r = 2r_0$  as a function of Strouhal number for (a) JetL6, (b) JetL8, (c) JetL10 and (d) JetL12.

impinges on the plate, and generates an acoustic wave propagating upstream towards the nozzle. This wave is then reflected by the nozzle lips, excites the shear layer, and leads to the formation of a new turbulent structure. The period of this feedback loop corresponds to the sum of the time necessary for a turbulent structure to travel downstream from the nozzle to the plate and the time of propagation of an acoustic wave from the plate to the nozzle, yielding the following relation<sup>2,3</sup>

$$\frac{L}{\langle u_c \rangle} + \frac{L}{a_0} = \frac{N}{f} \quad (1)$$

where  $\langle u_c \rangle$  is the mean convective velocity of the turbulent structures in the shear layers,  $a_0$  is the speed of sound outside of the jet, and the mode number  $N$  indicates the number of time the feedback mechanism occurs during one period.

The Strouhal numbers of the tone frequencies obtained for the present jets are shown in figure 10 as a function of the nozzle-to-plate distance. Only the fundamental tone frequencies, which are not harmonics of other tone frequencies and which will be called source tone frequencies in the following, are represented. The tone frequencies measured in the experiments of Krothapalli *et al.*<sup>5</sup>, as well as the tone frequencies predicted by the equation (1) using a mean value of convection velocity of  $\langle u_c \rangle = 0.60u_j$ , are also plotted.

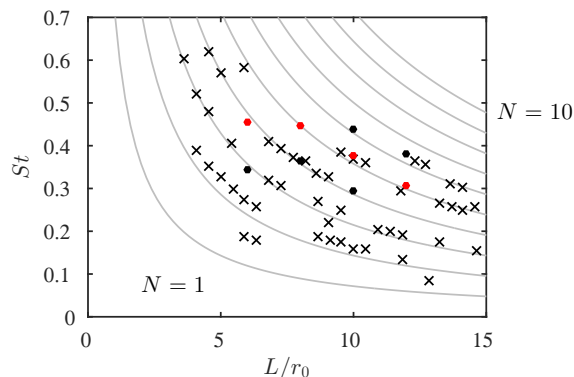


Figure 10. Representation of the Strouhal numbers of  $\bullet$  the dominant and  $\bullet$  the secondary tone frequencies obtained for the present jets, and  $\times$  tone frequencies found experimentally by Krothapalli *et al.*<sup>5</sup> for jets at similar conditions, as a function of the nozzle-to-plate distance  $L/r_0$ . The grey lines show the values predicted by equation (1) using  $u_c = 0.60u_j$ .

Overall, a good agreement is found between the simulation results and the experimental data of Krothapalli *et al.*<sup>5</sup> Moreover, the tone frequencies seem to be well predicted by equation (1). More precisely, the main tone frequencies are associated with the third and the fourth modes predicted by the model for JetL6, with the fourth and the fifth modes for JetL8, with the fourth, the fifth and the sixth modes for JetL10 and with the fifth and the sixth modes for JetL12. Moreover, the dominant tone frequency of JetL6 correspond to the fourth mode and the dominant tone frequencies of JetL8, JetL10 and JetL12 are all linked to the fifth mode. Such a staging behaviour of the dominant tone frequency with the nozzle-to-plate distance has been observed experimentally by Krothapalli<sup>25</sup> for a rectangular supersonic jet impinging on a flat plate. Besides, such a behaviour is typical of an aeroacoustic feedback mechanism, as that encountered in the oscillating flow over a cavity<sup>26</sup>.

## V. Study of the feedback mechanism

### V.A. Near pressure field

For each jet, the pressure field in the  $(z, r)$  plane has been recorded every  $50^{th}$  time step. The results are arranged in the  $M \times N$  matrix

$$P_{all} = \begin{bmatrix} P_1^1 & P_1^2 & \cdot & P_1^N \\ P_2^1 & P_2^2 & \cdot & P_2^N \\ \cdot & \cdot & \cdot & \cdot \\ P_M^1 & P_M^2 & \cdot & P_M^N \end{bmatrix} \quad (2)$$

where  $N$  is the number of samplings, and  $M = n_z \times 2n_r$  is the total number of points the  $(z, r)$  plane. The pressure field obtained at a given time is thus provided by one column of  $P_{all}$ . A Fast Fourier Transform is applied to each row of the matrix  $P_{all}$ . In this way, for a given frequency, the amplitude and phase fields can be displayed.

For the case  $L = 6r_0$ , the phase and the amplitude fields of the two main tone frequencies, at  $St_1 = 0.345$  and  $St_2 = 0.455$ , are displayed in figure 11. The results for the first tone, at  $St_1 = 0.345$ , are presented in figures 11(a,b). There is a 180 degree phase shift visible in the phase field with respect to the jet axis, indicating a sinuous or helical oscillation mode. More precisely, based on a Fourier decomposition of the fluctuating pressure on 32 sensors regularly spaced in the azimuthal direction at  $z = 0$  and  $r = 2r_0$ , the mode is helical. Moreover, a cell structure appear in the amplitude field. By considering the two semi-cells near the nozzle and the plate as one cell, this structure contains three cells. One can also note in figure 11(a) that the amplitude is strongly attenuated near the jet axis, as expected for an helical oscillation mode. The amplitude and phase fields for the second tone, at  $St_2 = 0.455$ , are shown in figures 11(c,d). This tone appears to be associated with an axisymmetric mode of the jet, and a cell structure is visible in the amplitude field between the nozzle and the plate.

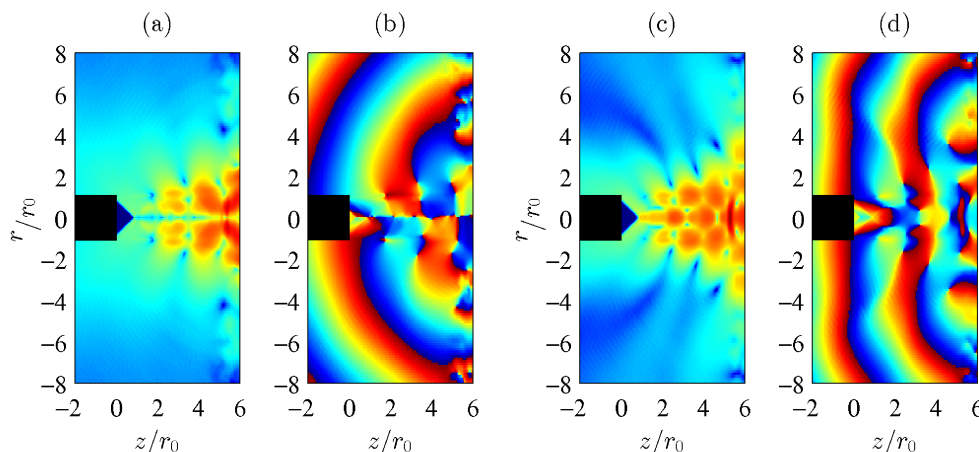


Figure 11. Amplitude and phase fields obtained for the two main tone frequencies of JetL6 (a,b) at  $St_1 = 0.345$  and (c,d) at  $St_2 = 0.455$ .

For the case  $L = 8r_0$ , the phase and the amplitude fields obtained for the two main tone frequencies at  $St_1 = 0.365$  and  $St_2 = 0.445$  are displayed in figure 12. The results for  $St_1 = 0.365$  are given in figures 12(a,b). In the phase field, there is no phase shift with respect to the jet axis, indicating that this tone is associated with an axisymmetric mode. Moreover, a cell structure containing four cells is visible in the jet in figure 12(a). The results for second tone at  $St_2 = 0.445$  are represented in figures 12(c,d). This tone is again related to an axisymmetric mode as there is no phase shift with respect to the jet axis in the phase field. The amplitude field exhibits a cell structure with five cells in the jet between the nozzle and the plate.

For the case  $L = 10r_0$ , the phase and the amplitude fields obtained for the three main tone frequencies are displayed in figure 13. The results for  $St_1 = 0.29$  are represented in figures 13(a,b). There is a 180 degree phase shift visible in the phase field with respect to the jet axis, indicating an helical oscillation mode. A structure containing four cells can be seen in the amplitude field. For  $St_2 = 0.375$ , there is no phase shift with respect to the jet axis in figure 13(d), supporting that this tone is associated with an axisymmetric mode. Moreover, a structure of five cells is visible in the jet in the amplitude field in figure 13(c). Finally, the results for  $St_3 = 0.44$  are given in figures 13(e,f). This tone appears to be linked to an axisymmetric oscillation mode, and a structure of six cells is noted in the amplitude field.

For the case  $L = 12r_0$ , the phase and the amplitude fields obtained for the two main tone frequencies at  $St_1 = 0.305$  and  $St_2 = 0.38$  are displayed in figure 14. The results for  $St_1 = 0.305$  are shown in figures 14(a,b). This tone is associated with an helical oscillation mode of the jet, and a structure containing five cells is observed in the amplitude field. For  $St_2 = 0.38$ , a structure of six cells is visible in the amplitude field and the phase field indicates an axisymmetric oscillation at this frequency.

The cell structures obtained in the amplitude fields are due to the presence of hydrodynamic-acoustic

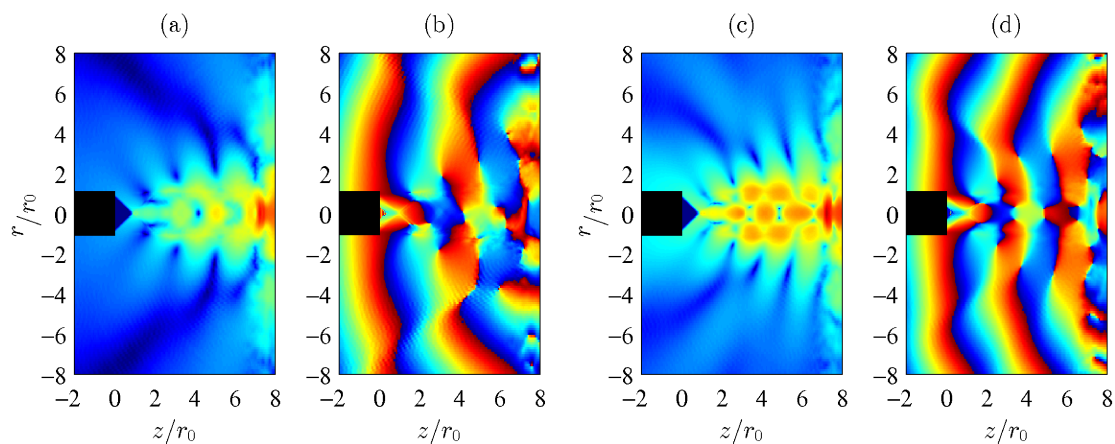


Figure 12. Amplitude and phase fields obtained for the two main tone frequencies of JetL8 (a,b) at  $St_1 = 0.365$  and (c,d) at  $St_2 = 0.445$ .

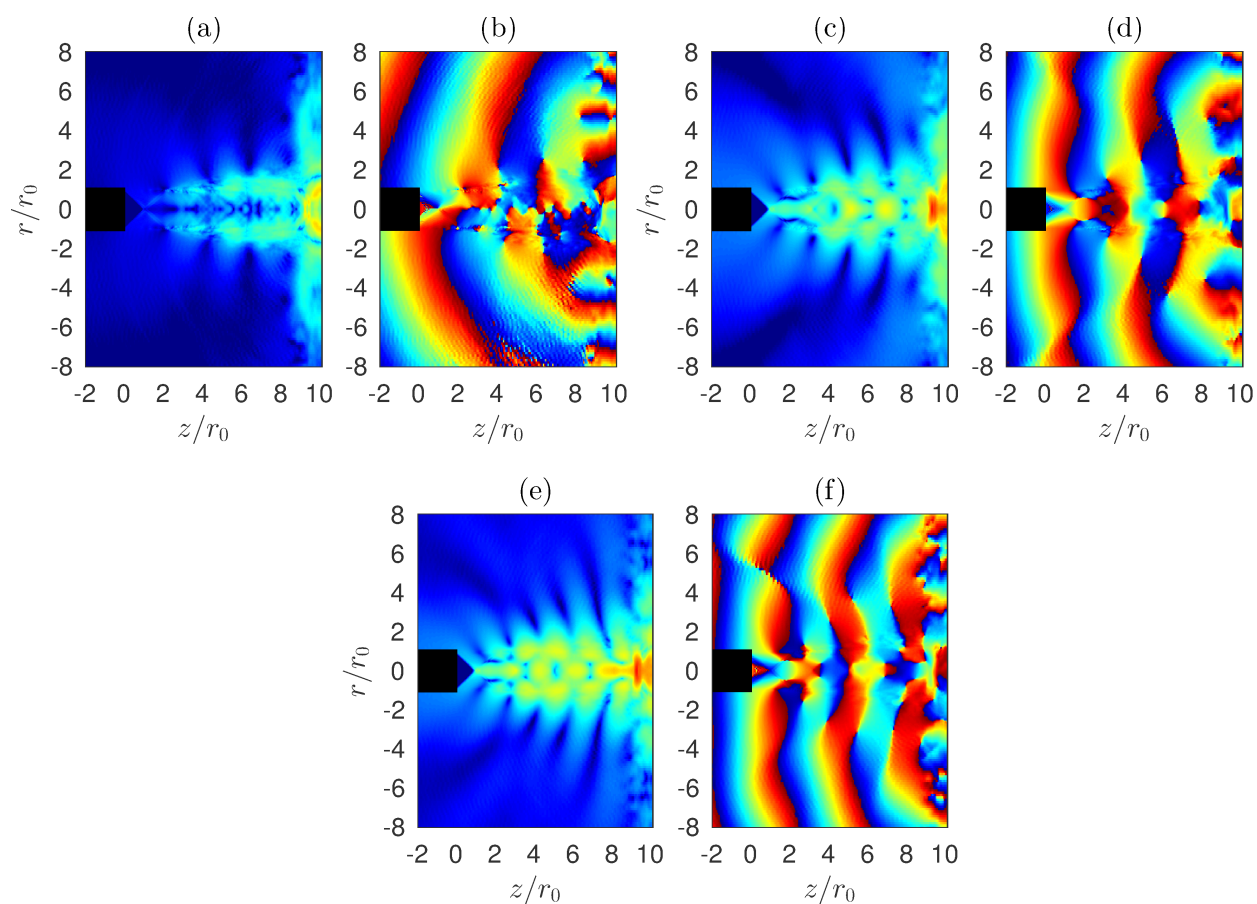


Figure 13. Amplitude and phase fields obtained for the two main tone frequencies of JetL10 (a,b) at  $St_1 = 0.29$ , (c,d) at  $St_2 = 0.375$  and (e,f) at  $St_3 = 0.44$ .

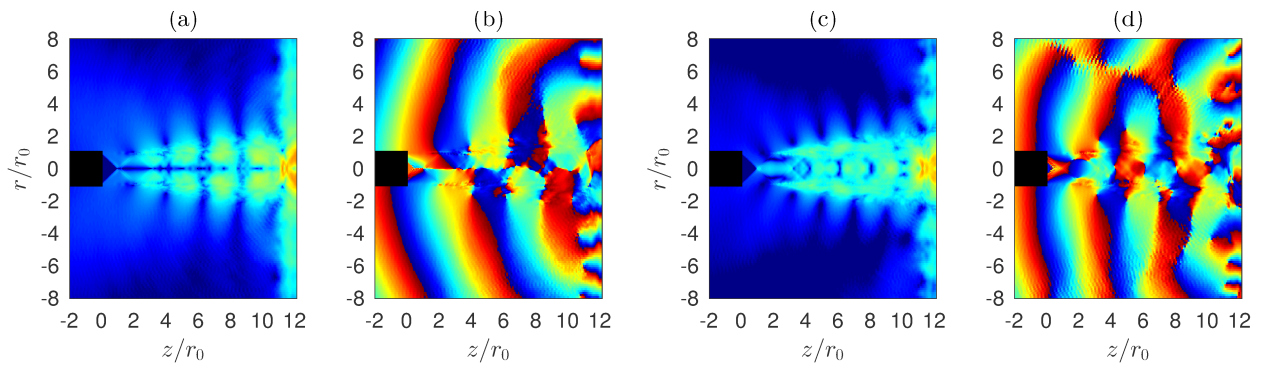


Figure 14. Amplitude and phase fields obtained for the two main tone frequencies of JetL12 (a,b) at  $St_1 = 0.305$  and (c,d) at  $St_2 = 0.38$ .

standing waves. Such structures were previously observed in Gojon *et al.*<sup>27</sup> for ideally expanded planar impinging jets. Gojon *et al.*<sup>27</sup> used the model of an hydrodynamic-acoustic standing wave proposed by Panda *et al.*<sup>28</sup> and showed that the number of cells in the standing wave is equal to the mode number. For all the tone frequencies considered above, the number of cells in the standing wave is indeed equal to the mode number. For example, in figure 11(a), there are three cells in the amplitude field of the dominant tone frequency of JetL6 at  $St_1 = 0.345$  and this tone corresponds in figure 10 to the third mode of the aeroacoustic feedback mechanism. Four cells are also visible in figure 11(c) in the amplitude field for the tone frequency at  $St_2 = 0.455$  of JetL6 and this tone is associated with the fourth mode of the feedback mechanism in figure 10.

### V.B. Vortex sheet model of a round jet

The results reported above concerning the jet oscillation modes associated with the tone frequencies of the feedback mechanism can be compared with the theoretical results of Tam and Ahuja<sup>29</sup>. These authors proposed that the upstream propagating waves of the feedback mechanism are associated with neutral acoustic wave modes of the vortex sheet model of the jet. Indeed, by considering a model with finite-thickness mixing layers, Tam and Hu<sup>30</sup> found three families of wave solutions, namely the Kelvin-Helmholtz instability wave modes which correspond to the vortical modes of the jet, and the supersonic and the subsonic instability waves which are the acoustic modes of the jet<sup>31–33</sup>. Tam and Norum<sup>12</sup> assumed that the acoustic waves of the feedback mechanism are related to the acoustic subsonic wave modes of the model with finite thickness mixing layers. These subsonic waves are found to be unstable in a model with finite-thickness mixing layers and neutral, with a real wave number  $k$ , in a vortex sheet model<sup>30</sup>. Thus, these waves have a real angular frequency  $\omega$  and, in a vortex sheet model, they have also a real wave number  $k$ .

A vortex sheet model is used to characterize the neutral acoustic wave modes of the present jet, as in the work of Tam and Norum<sup>12</sup> for planar jets and of Tam and Ahuja<sup>29</sup> for round jets. Here, an ideally expanded round jet of radius  $r_0$ , exit velocity  $u_j$  and Mach number  $\mathcal{M}_j$  is considered. The jet is bounded by a vortex sheet. A schematic representation of an axisymmetric instability of such a jet is given in figure 15.

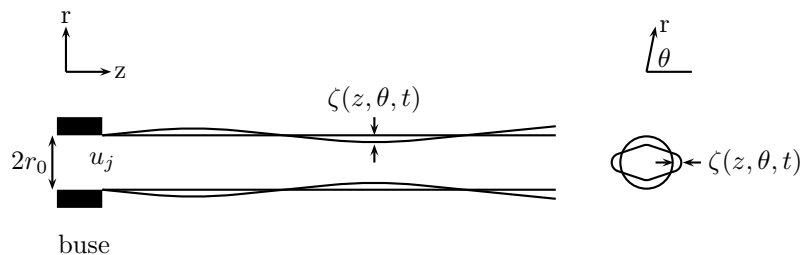


Figure 15. Axisymmetric instability of a round jet bounded by a vortex sheet.

The pressure fluctuations associated with the small-amplitude disturbances superimposed on the mean

flow inside and outside of the jet are denoted by  $p_{int}$  and  $p_{ext}$ , and the radial displacement of the vortex sheet is  $\zeta(z, \theta, t)$ . The linearised continuity, momentum and energy equations of a compressible inviscid fluid provide

$$\begin{cases} \Delta p_{ext} - \frac{1}{a_0^2} \frac{\partial^2 p_{ext}}{\partial t^2} = 0 \text{ outside the jet} \\ \Delta p_{int} - \frac{1}{a_j^2} \left( \frac{\partial^2 p_{int}}{\partial t^2} + u_j^2 \frac{\partial^2 p_{int}}{\partial z^2} \right) = 0 \text{ inside the jet} \end{cases} \quad (3)$$

where  $a_0$  and  $a_j$  are the sound speeds in the ambient medium and in the jet.

The boundary conditions on the vortex sheet, located at  $r = r_0$ , are

$$\begin{cases} p_{int} = p_{ext} \\ \frac{\partial^2 \zeta}{\partial t^2} = -\frac{1}{\rho_0} \frac{\partial p_{ext}}{\partial r} \\ \frac{\partial^2 \zeta}{\partial t^2} + u_j \frac{\partial^2 \zeta}{\partial z^2} = -\frac{1}{\rho_j} \frac{\partial p_{int}}{\partial r} \end{cases} \quad (4)$$

where  $\rho_0$  is the ambient density and  $\rho_j$  is the density in the jet.

The equation system (3) being closed, we can then look for wave solutions of the form

$$\begin{bmatrix} p_{int}(r, z, \theta, t) \\ p_{ext}(r, z, \theta, t) \\ \zeta(z, \theta, t) \end{bmatrix} = \begin{bmatrix} \hat{p}_{int}(r) \\ \hat{p}_{ext}(r) \\ \hat{\zeta} \end{bmatrix} e^{i(kz+n\theta-\omega t)} \quad (5)$$

where  $k$  and  $\omega$  are the wave number and the angular frequency of the wave. The system has been solved by Tam and Ahuja<sup>29</sup>. The following dispersion relation is found

$$\eta_+ J_n(\eta_- r_0) \frac{H_n^{1'}(\eta_+ r_0)}{H_n^1(\eta_+ r_0)} - \frac{a_j^2}{a_0^2} \frac{C^2}{(C - \mathcal{M}_j a_j / a_0)^2} \eta_- J_n'(\eta_- r_0) = 0 \quad (6)$$

where  $\eta_+ = (\omega^2/a_0^2 - k^2)^{1/2}$ ,  $\eta_- = [(\omega - u_j k)^2/a_j^2 - k^2]^{1/2}$ ,  $C = \omega/(ka_0)$ ,  $J_n$  is the  $n$ -th order Bessel function of the first kind, and  $H_n^1$  is the  $n$ -th order Hankel function of the first kind. A prime indicates the derivative.

For planar supersonic impinging jets, Tam and Norum<sup>12</sup> suggested that the acoustic waves of the feedback mechanism are related to the upstream propagating neutral acoustic wave modes of the vortex sheet model of the jet. Such waves have a wavenumber  $k$  and an angular frequency  $\omega$  which are both real. The relation (6) thus writes

$$|\xi_+| J_n(|\xi_- \alpha|) \frac{K_{n-1}(|\xi_+ \alpha|) + K_{n+1}(|\xi_+ \alpha|)}{K_n(|\xi_+ \alpha|)} + \frac{C^2 |\xi_-|}{(a_0 C / a_j - \mathcal{M}_j)^2} [J_{n-1}(|\xi_- \alpha|) - J_{n+1}(|\xi_- \alpha|)] = 0 \quad (7)$$

where  $\xi_+ = |C^2 - 1|^{1/2}$ ,  $\xi_- = |(a_0 C / a_j - \mathcal{M}_j)^2 - 1|^{1/2}$ ,  $\alpha = kr_0$ , and  $K_n$  is the  $n$ -th order modified Bessel function.

This dispersion relation is used in order to find the acoustic subsonic wave modes of the present jet. In this case, the nozzle have a diameter of  $D = 2$  mm and the jet Mach number is  $\mathcal{M}_j = 1.5$ . The dispersion relation is computed for the axisymmetric ( $n = 0$ ) and the helical ( $n = 1$ ) neutral acoustic wave modes and presented in figure 16 as functions of the wave number and the Strouhal number.

Four axisymmetric neutral acoustic wave modes of the vortex sheet model of the jet are found in figure 16(a). They are referred to as  $A1$ ,  $A2$ ,  $A3$  and  $A4$ . In the same way,  $H1$ ,  $H2$  and  $H3$  denote the three helical neutral acoustic wave modes visible in figure 16(b).

For Tam and Norum<sup>12</sup>, the acoustic waves of the feedback mechanism are linked to the upstream propagating neutral acoustic wave modes of the model. Obviously, they have a negative group velocity, that is

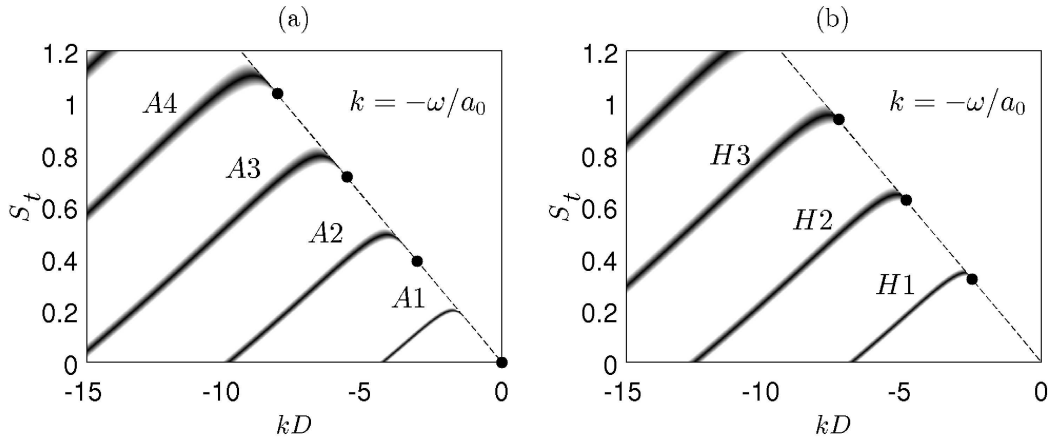


Figure 16. Dispersion relations of (a) axisymmetric and (b) helical neutral acoustic wave modes of the vortex sheet model for an ideally expanded jet with an exit diameter  $D = 2$  mm and a Mach number  $\mathcal{M}_j = 1.5$ ; • lower boundary of the modes; - - -  $k = -\omega/a_0$ .

to say  $d\omega/dk < 0$ . Such waves appear in figure 16, on the right hand side of each mode, where  $d\omega/dk$  is negative. Thus, allowable frequency ranges can be defined.

In order to determine the allowable frequency range of each mode, the two limits of the regions where  $d\omega/dk < 0$  are sought. The left hand side limits are picked on the graphs. On the right hand side, the lower boundaries can be calculated. Indeed, from equation (7), it is straightforward to note that the lower boundary of each mode is located on the dashed line plotted in figure 16, on which

$$k = -\frac{\omega}{a_0} \quad (8)$$

This line represents the upstream propagating neutral acoustic wave modes of the jet which have a group velocity of  $a_0$ .

For axisymmetric modes, for  $n = 0$ , when the wave number  $k$  tends to the value  $-\omega/a_0$ , relation (7) reduces to

$$\lim_{k \rightarrow -\omega/a_0} \frac{J_0(|\bar{\xi}_- \alpha|)}{|\alpha| \ln |\xi_+ \alpha|} + \frac{|\bar{\xi}_-|}{((a_0/a_j) + \mathcal{M}_j)^2} J_1(|\bar{\xi}_- \alpha|) = 0 \quad (9)$$

where  $\bar{\xi}_- = |(a_0/a_j + \mathcal{M}_j)^2 - 1|^{1/2}$ .

For the first axisymmetric mode A1, Tam et al. <sup>29</sup> showed that  $St$  tends to 0 when  $\alpha = kr_0 = kD/2$  tends to 0. The lower boundary of mode A1 is thus  $(St, kD) = (0, 0)$ . For the axisymmetric modes A2, A3, ..., the lower boundaries are given by

$$St_{Ai}^{min} = \frac{\sigma_i}{\pi \mathcal{M}_j (a_j/a_0) |(a_0/a_j + \mathcal{M}_j)^2 - 1|^{1/2}} \quad (10)$$

where  $\sigma_i$  is the  $i$ -th root of  $J_1$ .

For helical modes, for  $n = 1$ , when the wave number  $k$  tends to  $-\omega/a_0$ , relation (7) gives

$$2J_1(|\bar{\xi}_- \alpha|) + \frac{|\bar{\xi}_- \alpha|}{((a_0/a_j) + \mathcal{M}_j)^2} (J_0(|\bar{\xi}_- \alpha|) - J_2(|\bar{\xi}_- \alpha|)) = 0 \quad (11)$$

For each mode H1, H2 and H3, the solution of relation (11) is calculated. The values found from equations (10) and (11) have been shown in figure 16. The allowable frequency ranges of each upstream propagating neutral acoustic wave modes are represented in figure 17 for the axisymmetric and helical modes as a function of the exit Mach number  $\mathcal{M}_j$ . The nine dominant tones of the simulated jets are also plotted, depending on their axisymmetric or helical nature. The six tones associated with axisymmetric oscillation modes are located in the second axisymmetric allowable band given by the model or just below. The three dominant tones linked to helical oscillation modes fall into the first helical allowable band given by the model or just below. A similar result was found by Tam and Norum <sup>12</sup> for planar ideally expanded impinging jets

using a 2-D vortex sheet model of a jet. Therefore, the model seems to well predict the nature of the jet oscillation modes associated with the aeroacoustic feedback mechanism.

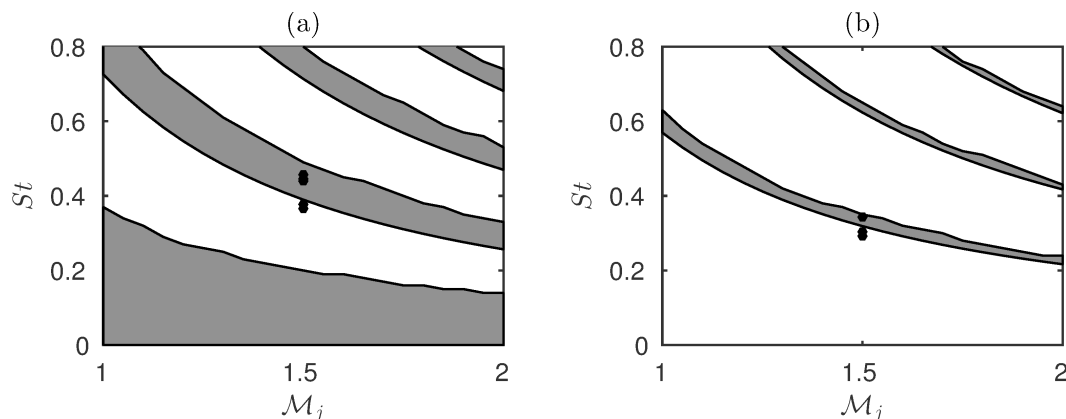


Figure 17. Allowable frequency ranges of the (a) axisymmetric and (b) helical upstream propagating neutral acoustic wave modes of the vortex sheet model of a round ideally expanded jet as a function of the jet exit Mach number.

## VI. Conclusion

In this paper, the hydrodynamic and acoustic properties of four supersonic round impinging jets computed by compressible large-eddy simulations using low-dissipation schemes are presented. The jets are ideally expanded, they have a Mach number of  $\mathcal{M}_j = 1.5$ , and a Reynolds number of  $Re_j = 6 \times 10^4$ . Mean velocity flows and snapshots of density and fluctuating pressure are described. The development of the shear layers is investigated by computing the rms values of velocity fluctuations and the convection velocities of turbulent structures. The near pressure fields are then detailed. The pressure spectra in the vicinity of the nozzle show several emerging tones, which agree well with the measurements of Krothapalli *et al.*<sup>5</sup>, as well as with the model of Ho and Nosseir<sup>2</sup>. A Fourier decomposition is applied to the pressure fields in the  $(z, r)$  plane. The amplitude and the phase fields obtained for the dominant tone frequencies in each case are determined. The amplitude fields reveal the presence of an hydrodynamic-acoustic standing wave for each source tone frequency, as observed by Panda *et al.*<sup>28</sup> in screeching supersonic jets. The number of cells in the standing wave structure corresponds to the mode number in the model of Ho and Nosseir<sup>2</sup>, as previously noted in Gojon *et al.*<sup>27</sup> for planar ideally expanded supersonic impinging jets. The phase fields obtained at the different tone frequencies provide the axisymmetric or helical nature of the corresponding modes. Finally, the theoretical developments of Tam and Norum<sup>12</sup> based on a vortex sheet model of the jet are used. This model is shown to well predict the nature of the jet oscillation modes associated with the aeroacoustic feedback mechanism.

## Acknowledgments

This work was performed using HPC resources of P2CHPD (Pôle de Calcul Hautes Performances Dédiés) and IDRIS (Institut du Développement et des Ressources en Informatique Scientifique) under the allocation 2015-2a0204 made by GENCI (Grand Equipement National de Calcul Intensif). This work was performed within the framework of the Labex CeLyA of Université de Lyon, within the program "Investissements d'Avenir" (ANR-10-LABX-0060/ ANR-11-IDEX-0007) operated by the French National Research Agency (ANR).

## References

- <sup>1</sup> A. Powell. On edge tones and associated phenomena. *Acta Acust. United Ac.*, 3:233–243, 1953.
- <sup>2</sup> C.M. Ho and N.S. Nosseir. Dynamics of an impinging jet. part 1. the feedback phenomenon. *J. Fluid Mech.*, 105:119–142, 1981.

- <sup>3</sup> N.S. Nosseir and C.M. Ho. Dynamics of an impinging jet. part 2. the noise generation. *J. Fluid Mech.*, 116:379–391, 1982.
- <sup>4</sup> B. Henderson and A. Powell. Experiments concerning tones produced by an axisymmetric choked jet impinging on flat plates. *J. Sound Vib.*, 168(2):307–326, 1993.
- <sup>5</sup> A. Krothapalli, E. Rajkuperan, F. Alvi, and L. Lourenco. Flow field and noise characteristics of a supersonic impinging jet. *J. Fluid Mech.*, 392:155–181, 1999.
- <sup>6</sup> B. Henderson, J. Bridges, and M. Wernet. An experimental study of the oscillatory flow structure of tone-producing supersonic impinging jets. *J. Fluid Mech.*, 542:115–137, 2005.
- <sup>7</sup> A. Risborg and J. Soria. High-speed optical measurements of an underexpanded supersonic jet impinging on an inclined plate. *28th International Congress on High-Speed Imaging and Photonics*, 7126(F), 2009.
- <sup>8</sup> N.A. Buchmann, D.M. Mitchell, K.M. Ingvorsen, D.R. Honnery, and J. Soria. High spatial resolution imaging of a supersonic underexpanded jet impinging on a flat plate. *6th Australian Conference on Laser Diagnostics in Fluid Mechanics and Combustion*, 2011.
- <sup>9</sup> D.M. Mitchell, D.R. Honnery, and J. Soria. The visualization of the acoustic feedback loop in impinging underexpanded supersonic jet flows using ultra-high frame rate schlieren. *J. of visualization*, 15(4):333–341, 2012.
- <sup>10</sup> T. Davis, A. Edstrand, F. Alvi, L. Cattafesta, D. Yorita, and K. Asai. Investigation of impinging jet resonant modes using unsteady pressure-sensitive paint measurements. *Exp. in Fluids*, 56(5):1–13, 2015.
- <sup>11</sup> T.D. Norum. Supersonic rectangular jet impingement noise experiments. *AIAA J.*, 29(7):1051–1057, 1991.
- <sup>12</sup> C.K.W. Tam and T.D. Norum. Impingement tones of large aspect ratio supersonic rectangular jets. *AIAA J.*, 30(2):304–311, 1992.
- <sup>13</sup> K. Hourigan, M. Rudman, and E. Brocher. The feedback loop in impinging two-dimensional high-subsonic and supersonic jets. *Experimental thermal and fluid science*, 12(2):265–270, 1996.
- <sup>14</sup> C. Bogey, O. Marsden, and C. Bailly. Large-eddy simulation of the flow and acoustic fields of a reynolds number  $10^5$  subsonic jet with tripped exit boundary layers. *Phys. Fluids*, 23:035104, 2011.
- <sup>15</sup> C. Bogey and C. Bailly. A family of low dispersive and low dissipative explicit schemes for flow and noise computations. *J. Comput. Phys.*, 194(1):194–214, 2004.
- <sup>16</sup> J. Berland, C. Bogey, O. Marsden, and C. Bailly. High-order, low dispersive and low dissipative explicit schemes for multiple-scale and boundary problems. *J. Comput. Phys.*, 224(2):637–662, 2007.
- <sup>17</sup> C.K.W. Tam and Z. Dong. Wall boundary conditions for high-order finite-difference schemes in computational aeroacoustics. *Theor. Comput. Fluid Dyn.*, 6:303–322, 1994.
- <sup>18</sup> C. Bogey, N. de Cacqueray, and C. Bailly. A shock-capturing methodology based on adaptative spatial filtering for high-order non-linear computations. *J. Comput. Phys.*, 228(5):1447–1465, 2009.
- <sup>19</sup> N. de Cacqueray, C. Bogey, and C. Bailly. Investigation of a high-mach-number overexpanded jet using large-eddy simulation. *AIAA J.*, 49(10):2171–2182, 2011.
- <sup>20</sup> K. Mohseni and T. Colonius. Numerical treatment of polar coordinate singularities. *J. Comput. Phys.*, 157(2):787–795, 2000.
- <sup>21</sup> C. Bogey, N. de Cacqueray, and C. Bailly. Finite differences for coarse azimuthal discretization and for reduction of effective resolution near origin of cylindrical flow equations. *J. Comput. Phys.*, 230(4):1134–1146, 2011.
- <sup>22</sup> R. Gojon, C. Bogey, and O. Marsden. Large-eddy simulation of underexpanded round jets impinging on a flat plate 4 to 9 radii downstream from the nozzle. *AIAA Paper 2015-2210*, 2015.

- <sup>23</sup> H.P.A.H. Irwin. Measurements in a self-preserving plane wall jet in a positive pressure gradient. *J. Fluid Mech.*, 61(01):33–63, 1973.
- <sup>24</sup> W.K. George, H. Abrahamsson, J. Eriksson, R.I. Karlsson, L. Löfdahl, and M. Wosnik. A similarity theory for the turbulent plane wall jet without external stream. *J. Fluid Mech.*, 425:367–411, 2000.
- <sup>25</sup> A. Krothapalli. Discrete tones generated by an impinging underexpanded rectangular jet. *AIAA J.*, 23(12):1910–1915, 1985.
- <sup>26</sup> D. Rockwell and E. Naudascher. Review-self-sustaining oscillations of flow past cavities. *J. Fluids Engineering*, 100(2):152–165, 1978.
- <sup>27</sup> R. Gojon, C. Bogey, and O. Marsden. Large-eddy simulation of supersonic planar jets impinging on a flat plate at an angle of 60 to 90 degrees. *AIAA Paper 2015-2209*, 2015.
- <sup>28</sup> J. Panda, G. Raman, and K.B.M.Q. Zaman. Underexpanded screeching jets from circular, rectangular and elliptic nozzles. *AIAA Paper 97-1623*, 1997.
- <sup>29</sup> C.K.W. Tam and K.K. Ahuja. Theoretical model of discrete tone generation by impinging jets. *J. Fluid Mech.*, 214:67–87, 1990.
- <sup>30</sup> C.K.W. Tam and F.Q. Hu. On the three families of instability waves of high-speed jets. *J. Fluid Mech.*, 201:447–483, 1989.
- <sup>31</sup> C.H. Berman and J.E. Williams. Instability of a two-dimensional compressible jet. *J. Fluid Mech.*, 42(01):151–159, 1970.
- <sup>32</sup> L.M. Mack. On the inviscid acoustic-mode instability of supersonic shear flows. *Theor. Comput. Fluid Dyn*, 2(2):97–123, 1990.
- <sup>33</sup> R. Sabatini and C. Bailly. Numerical algorithm for computing acoustic and vortical spatial instability waves. *AIAA J.*, 53(3):692–702, 2014.